ACS OMEGA

http://pubs.acs.org/journal/acsodf

Article

Spectroscopic Study of the $B\ ^1\Pi$ State of NaH

Chia-Ching Chu, Chun Huang, Chin-Chun Tsai,* and Thou-Jen Whang*

Cite This: *ACS Omega* 2021, 6, 20629−20636

Read Online

ACCESS | Metrics & More | Article Recommendations | Supporting Information

ABSTRACT: In this study, the $B\ ^1\Pi$ excited state of NaH has been experimentally studied for the first time. Pulsed laser-induced fluorescence excitation spectroscopy was used to investigate the $B\ ^1\Pi$ electronic state of NaH. A total of 48 ro-vibronic transitions were observed, including within the $B-X\ (0-0)$ and $B-X\ (0-1)$ transition bands. Only one B-state vibrational level was identified, and a series of PQR lines, with eight e-parity and eight f-parity sublevels ($v' = 0$, $J' = 1-8$), were assigned. The level assignment was supported by a comparison of the experimental line positions with the *ab initio* calculations, the dispersed laser-induced fluorescence spectrum of the NaH $B\ ^1\Pi \rightarrow X\ ^1\Sigma^+$ emission, and the V-type optical−optical double resonance spectra. The Dunham-type coefficients, the mean internuclear distance, the harmonic vibrational frequency ω, and the dissociation energies D_0 and D_e of the $B\ ^1\Pi$ state were determined.

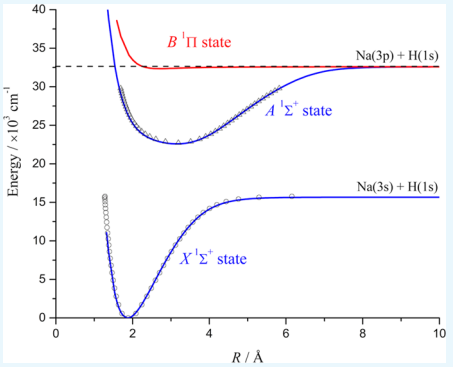

1. INTRODUCTION

Sodium hydride and sodium deuteride have attracted the interest of theoretical and experimental research since the 1930s. Because of their hydrogen-like electronic states, which have been analyzed thoroughly for many years, scientists have paid an effort to reach their electronic idiosyncrasies. The combination of a gaseous hydrogen (or its isotope, deuterium) atom and a gaseous sodium atom will result in various electronic states, with each presenting different behavior of potential energy curves based on the different angular momentums, spin angular momentums, and magnetic spin quantum number couplings.[1] A comprehensive spectroscopic review of alkali hydride diatomic molecules has been presented.[2] Until now, only a few electronic states have been experimentally observed and reported: $X\ ^1\Sigma^+$,[3,4] $A\ ^1\Sigma^+$,[5,6] and $C\ ^1\Sigma^+$[7,8] states. The NaH $B\ ^1\Pi$ state has been studied theoretically for decades, and many of the calculated results indicate that it is a bound state.[9−19] However, no experimental observation of this state has been reported to date. The $B\ ^1\Pi$ state is a weakly bound state with a binding energy of less than 300 cm^{-1};[19] this shallow potential energy can sustain only three (NaH) or four (NaD) rotationless vibrational levels. The data of a weakly bound state is usually insufficient.[20] Due to the shallow potential well and poor Franck−Condon overlap,[1] the rovibrational level of a weakly bound state is hard to be observed using the laser method. Many theoretical calculations have been done to estimate the behavior inside a weakly bound state.[19−23] These calculations helped us to predict the transition of rovibrational levels in laser spectroscopy. However, some experimental results of weakly bound states showed a quite large difference compared to the corresponding theoretical calculation.[24−26] Thus, the experimental study of weakly bound states makes rectification of the difference between theoretical calculations and experimentally observed signals.

The electronic states of alkali hydrides (LiH to CsH) showed similar trends, and the systematic trends in electronic properties of alkali hydrides had been researched thoroughly,[19] in which the $B\ ^1\Pi$ state of alkali hydrides (LiH to RbH) presented weakly bound state property. In the aspect of the experiment, the $B\ ^1\Pi$ state of LiH and KH had been observed.[26−28] The molecular constants of KH calculated from experimental data showed a large difference with theoretical calculations. Figure 1 plots the two lowest $^1\Sigma^+$ states and the first $^1\Pi$ state of the NaH molecule; the solid lines denote the *ab initio* potential energy curves,[19] the open circles and open triangles represent the Rydberg−Klein−Rees potential energy curves adopted from the experimental works,[3,6] and the dashed line represents the energy of the $Na(3\ ^2P_{3/2}) + H(1\ ^2S_{1/2})$ asymptote. The present study is the first to provide spectroscopic results for the NaH $B\ ^1\Pi$ state. This state was investigated using laser-induced fluorescence (LIF) excitation spectroscopy. The $B\ ^1\Pi-X\ ^1\Sigma^+$ band system of sodium hydride is located in a wavelength region of the second harmonic generation of a tunable dye laser with the DCM dye. In this wavelength region, signals of other sodium dimers also appeared in the LIF spectra, which severely interfered with the determination of the NaH B state. The deduction of sodium

Received: May 30, 2021
Accepted: July 16, 2021
Published: July 28, 2021

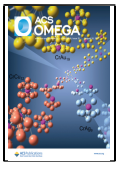

https://doi.org/10.1021/acsomega.1c02767
ACS Omega 2021, 6, 20629−20636

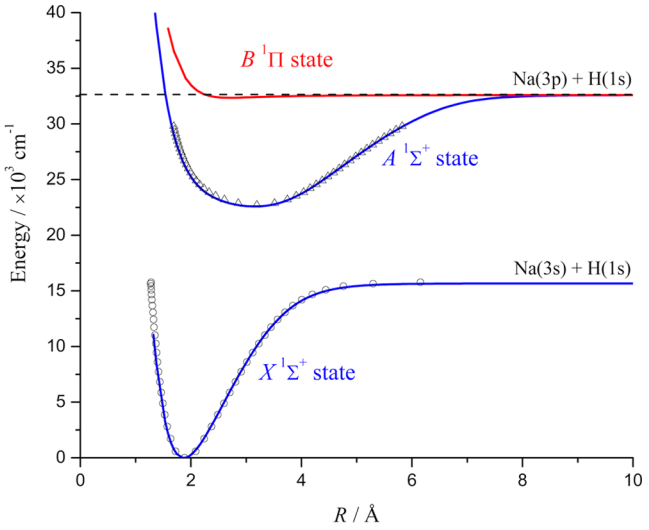

Figure 1. Ground state and first excited singlet state and the target state $B\ ^1\Pi$ of the NaH molecule (solid blue and red lines denote values from Aymar et al.,[19] open circles denote values from Huang et al.,[3] and open triangles denote values from Pesl et al.[6]). The black dashed line represents the Na($3\ ^2P_{3/2}$) + H ($1\ ^2S_{1/2}$) asymptote.

dimer signals was also performed. In our investigation, only one excited-state vibrational level ($v = 0$) was observed due to poor Franck−Condon overlap between the higher vibrational levels of the NaH B state (where $v = 1$ and $v = 2$) and the thermally populated ground state ($v'' = 0$ and 1). A total of 48 $B\ ^1\Pi \leftarrow X\ ^1\Sigma^+$ ro-vibronic transitions were observed, including eight e-parity and eight f-parity sublevels. The vibrational progressions were characterized through a comparison of the experimental data with the *ab initio* calculations,[19] and the rotational quantum numbers were assigned and verified by the LIF spectra and V-type optical−optical double resonance (OODR) spectroscopy results. The Dunham expansion was used to fit the observed rovibrational levels, and the dissociation energy of the NaH B state was estimated.

2. EXPERIMENTAL SETUP

Figure 2 illustrates the experimental setup of the present study. The second harmonic of a pulsed Nd:YAG laser (Continuum Powerlite 8000) was used as a pump source for pumping a dye laser (Lambda Physik Scanmate II). The Nd:YAG laser had a repetition rate of 10 Hz, and its pulse width was 5−7 ns, with an energy per pulse of approximately 50 mJ. The dye laser was operated with a methanol solution of DCM dye, and the

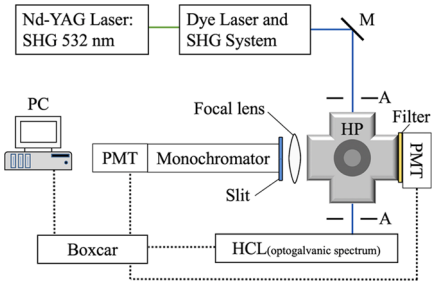

Figure 2. Block diagram of the experimental setup. SHG, second harmonic generation; M, mirror; HP, heat pipe oven; A, aperture; PMT, photomultiplier tube; HCL, hollow cathode lamp; PC, personal computer.

linewidth was approximately 0.15 cm^{-1}. A frequency doubling system (BBO III crystal) was used to generate an ultraviolet laser beam to investigate the NaH $B\ ^1\Pi$ state. The frequency-doubled dye laser was calibrated according to the optogalvanic spectrum of the Fe−Ne hollow cathode lamp (Hamamatsu L233-26NU, Hamamatsu, Japan). The absolute energy of neon atomic lines was obtained from a previous study,[29] and the accuracy of the calibration was approximately 0.1 cm^{-1}.

Sodium hydride vapor was generated using a five-arm stainless steel heat pipe system that was loaded with a sufficient amount of sodium metal, prepurged with hydrogen gas, filled with approximately 1 Torr of argon buffer gas, and heated to approximately 390 °C. The dye laser beam was aligned along the longer arms of the heat pipe, and fluorescence measurements were obtained from the perpendicular shorter arms. A monochromator with a 0.05 nm resolution (Acton Research Corporation SP-500, Acton) equipped with a photomultiplier tube (Hamamatsu R928, Hamamatsu, Japan) was used to detect the signals of the fluorescence excitation spectrum and LIF spectrum. Filters (Schott KV470) were paired with the photomultiplier tubes and placed at the opposite sides of the shorter arms to detect the fluorescence of both the sodium dimer and sodium hydride.

In the present study, the time sequence of the dye laser was synchronized with that of the Nd:YAG laser and monitored on a digital oscilloscope (LeCroy 9361). We used a three-channel boxcar integrator (Stanford Research Systems SR245, SR250, and SR280) to simultaneously monitor the signals of the fluorescence excitation spectra, the filter/photomultiplier measurements, and the optogalvanic spectra. The outputs of the boxcars were processed and recorded using a personal computer.

3. RESULTS AND DISCUSSION

3.1. Spectra and Assignment. We derived the expected rovibrational levels of the NaH $B\ ^1\Pi$ state from theoretical calculations by solving Hamiltonian equations with the potential energy curve provided by Aymar et al.[19] The calculation results indicated that the NaH B state had only three bound vibrational levels. The expected PQR line positions of the NaH $B\ ^1\Pi \leftarrow X\ ^1\Sigma^+$ transitions were calculated with reference to the works of Huang et al.[3] ($X\ ^1\Sigma^+$ state) and Aymar et al.[19] ($B\ ^1\Pi$ state). The calculation results indicated that the fluorescence excitation spectra should be experimentally observed in the spectral range of approximately (a) 31 700−32 200 cm^{-1} excited from the ground state, where $v'' = 0$, and (b) 30 600−31 100 cm^{-1} excited from the ground state, where $v'' = 1$.

The fluorescence excitation spectra of the NaH $B\ ^1\Pi$ state were obtained using pulsed LIF excitation spectroscopy.[30] Second harmonic pulsed dye laser excitation was applied to observe the fluorescence of NaH and Na_2 molecules with a photomultiplier through a Schott KV470 filter. To avoid the interference of Na_2 fluorescence, the fluorescence signal of the NaH B state was recorded through a monochromator at 388 or 403 nm in accordance with the $B(0)−X(6)$ or $B(0)−X(7)$ vibrational band of NaH, respectively. The detection wavelength window was selected in accordance with predictions of the NaH B state LIF bands.

Although the fluorescence excitation spectra could be observed through different monochromator settings (at 388 or 403 nm; slit width of 1.5−3.0 mm), the acquired spectra had the same PQR line positions but different intensities.

https://doi.org/10.1021/acsomega.1c02767
ACS Omega 2021, 6, 20629−20636

Figure 3 illustrates the fluorescence excitation spectrum of the NaH B state excited from X (v'' = 0, J'') along with its assignments. Only one vibrational level was found in this study, possibly due to the lack of Franck−Condon overlap, which would have been used to experimentally observe the higher vibrational levels. The vibrational quantum number v of the observed ground-state vibrational level was assigned to a value of 0 on the basis of a comparison between the experimentally observed data and the calculation results.[19] The left two columns of Table 1 list the term values of the 24 discernible transitions that were identified (see the Supporting Information). The rotational quantum number J was assigned on the basis of a comparison between the experimental ro-vibronic line positions and the calculation results,[19] and the LIF spectrum of each $B \leftarrow X$ transition was individually recorded to confirm that the calculated LIF spectral bands matched the observed fluorescence peaks (see Section 3.2).

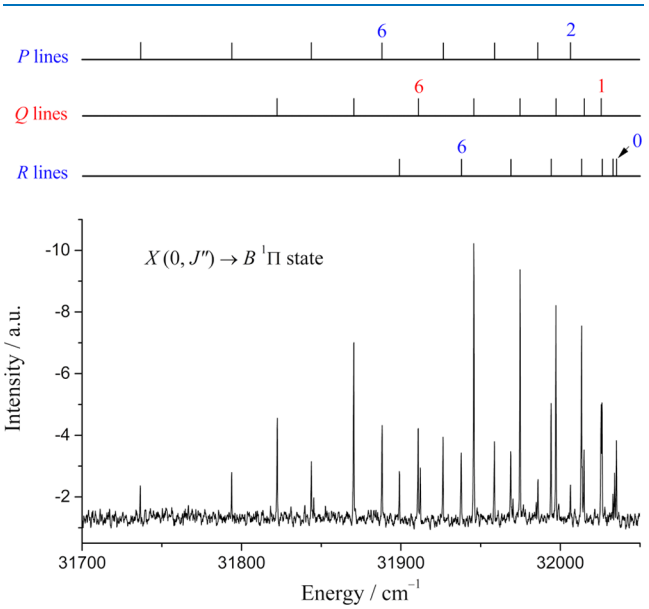

Figure 3. Experimentally recorded dispersed laser-induced fluorescence excitation spectrum of the $X(0)-B(0)$ vibrational band of NaH (lower graph) and the assignment of PQR lines (upper graph).

The B (0, J) ← X (1, J'') transitions were estimated quite accurately from the term values of the NaH B state, which were determined according to the B (0, J) ← X (0, J'') transitions (see the left two columns of Table 1). The same method mentioned in the last paragraph was employed to observe the fluorescence excitation spectrum of the NaH B state excited from X (1, J''). However, the excitation fluorescence of the sodium dimer could not be avoided in the scanning range of 30 600−30 925 cm^{-1}, even when the monochromator was set to different wavelength windows (see Figure 4b). Fortunately, difference spectral analysis eliminated the interference of the sodium dimer. The excitation fluorescence spectrum of the

Table 1. Observed Term Values of the NaH B State for the Vibrational Quantum Number v = 0: (a) e Sublevels of P and R Lines and (b) f Sublevels of Q Lines[a]

(a) e-parity sublevels (P and R lines)				
B (0, $''J$) ← X (0, J'')	term value/cm^{-1}	J	term value/cm^{-1}	B (0, $''J$) ← X (1, J'')
$R(0)$	32616.1402	1	32615.3421	$R(0)$
$P(2)$	32616.1969	1	32616.5091	$P(2)$
$R(1)$	32623.4392	2	32623.6884	$R(1)$
$P(3)$	32624.7708	2	32624.6513	$P(3)$
$R(2)$	32635.8763	3	32635.5019	$R(2)$
$P(4)$	32635.9333	3	32636.2709	$P(4)$
$R(3)$	32652.1092	4	32651.5376	$R(3)$
$P(5)$	32651.9308	4	32651.4599	$P(5)$
$R(4)$	32671.6159	5	32671.4976	$R(4)$
$P(6)$	32671.4307	5	32671.6338	$P(6)$
$R(5)$	32694.3873	6	32694.4162	$R(5)$
$P(7)$	32694.2261	6	32694.0364	$P(7)$
$R(6)$	32721.0257	7	32721.0425	$R(6)$
$P(8)$	32720.9205	7	32721.0235	$P(8)$
$R(7)$	32749.4817	8	32749.2758	$R(7)$
$P(9)$	32749.4894	8	32749.1039	$P(9)$
(b) f-parity sublevels (Q lines)				
B (0, $''J$) ← X (0, J'')	**term value/cm^{-1}**	**J**	**term value/cm^{-1}**	**B (0, $''J$) ← X (1, J'')**
$Q(1)$	32616.1560	1	32616.7154	$Q(1)$
$Q(2)$	32624.7012	2	32623.7599	$Q(2)$
$Q(3)$	32636.1305	3	32636.0866	$Q(3)$
$Q(4)$	32652.0777	4	32652.2557	$Q(4)$
$Q(5)$	32671.5121	5	32671.6877	$Q(5)$
$Q(6)$	32694.0196	6	32693.6158	$Q(6)$
$Q(7)$	32720.9158	7	32721.2529	$Q(7)$
$Q(8)$	32749.3492	8	32748.9102	$Q(8)$

[a]The first and fourth columns list values within the $X(0)-B(0)$ and $X(1)-B(0)$ transition bands, respectively; J'' is the rotational quantum number of the ground state and is used for the notation of $P(J'')$, $Q(J'')$, and $R(J'')$ lines. The second and third columns are the term values of the rovibrational state B (0, J) with different values for the rotational quantum number J.

https://doi.org/10.1021/acsomega.1c02767
ACS Omega 2021, 6, 20629−20636

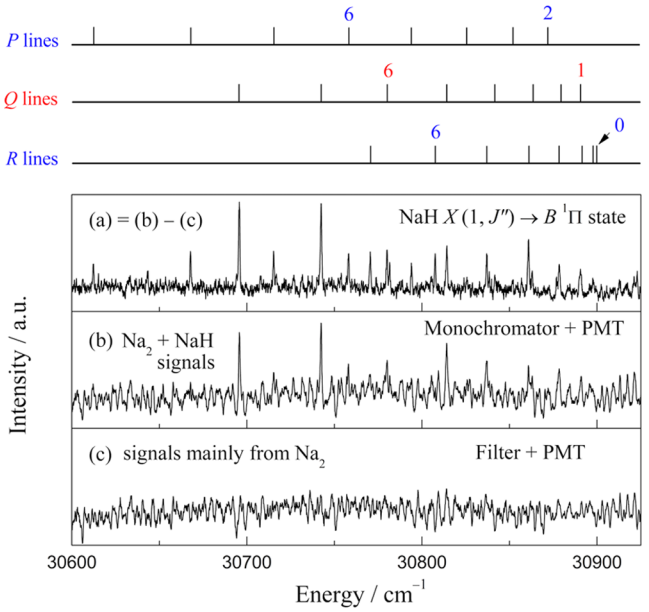

Figure 4. Lower half: (a) difference spectrum of the $X(1)-B(0)$ vibrational band of NaH, (b) experimentally recorded dispersed laser-induced fluorescence excitation spectrum of Na_2 and NaH, and (c) excitation spectrum of Na_2. Upper half: assignment of PQR lines of the $X(1)-B(0)$ vibrational band.

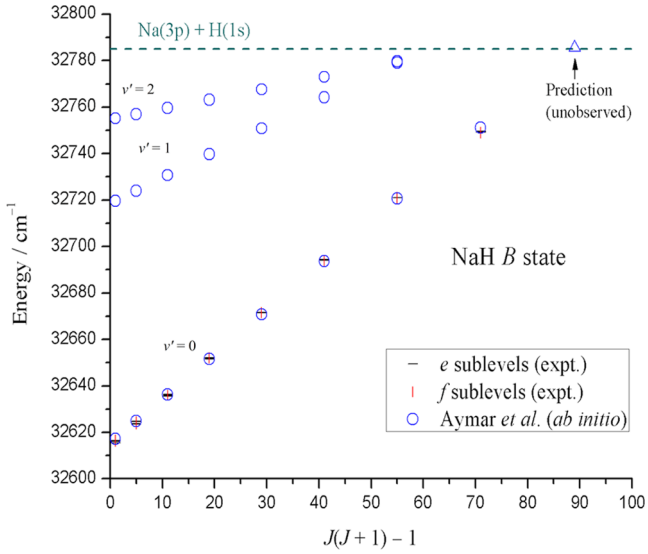

Figure 5. Plot of the term values $T(v, J)$ versus $[J(J + 1) - 1]$. The black horizontal dashes represent the *e* sublevels, and the red vertical dashes represent the *f* sublevels. The hollow blue circles represent eigenvalues from Aymar et al.[19] The hollow blue triangle denotes a predicted level that was not observed in this work. The dashed green line represents the dissociation limit.

sodium dimer was recorded with a filter/photomultiplier combination (see Figure 4c) that also contained sodium hydride's relatively weak fluorescence signal. Figure 4a shows the difference spectrum, which contained clear fluorescence signals of the NaH *B* state. The term values are listed in the right two columns of Table 1, and the transition energies of the $X(0)-B(0)$ and $X(1)-B(0)$ transition bands are presented in the Supporting Information.

Figure 5 plots the term values $T(v, J)$ versus $[J(J + 1) - 1]$ of three vibrational levels of the NaH *B* state. The black horizontal and red vertical dashes represent the experimental rovibrational levels where $v = 0$, including the *e* and *f* sublevels. According to ref 1, the magnitude of Λ-type doubling amounts to only a few cm^{-1}, close to that of our experimental resolution; therefore, the Λ doubling splitting was ambiguous and could not be distinguished, as illustrated in Figure 5.

The blue open circles in Figure 5 represent the rovibrational levels derived from solving Hamiltonian equations using the *ab initio* potential energy curve.[19] The calculated levels derived from the *ab initio* potential curve were offset to agree with the experimental levels, and the trends are in good agreement with each other. The energy of the asymptote, Na(3p) + H(1s) = 32 785(6) cm^{-1}, was estimated using the dissociation energy $D_e(X)$ = 15 812(6) cm^{-1} for the NaH ground state[4] and the atomic energy difference $\Delta E[Na(3\ ^2P_{3/2}) - Na(3\ ^2S_{1/2})]$ = 16973.366 19(5) cm^{-1}.[31] The predicted rovibrational level *B* $^1\Pi$ ($v' = 0$, $J' = 9$) [also *B* (0, 9), as used in the rest of this article], which is slightly higher than the dissociation limit, was estimated using the extrapolation method (see the blue triangle in Figure 5), and the two vibrational states ($v = 1$ and 2) were predicted to exist in the NaH *B* state due to the *ab initio* potential energy curve. However, we observed no distinguishable signals after carefully surveying the predicted frequency range of these transitions.

For estimating the rovibrational levels of the NaD *B* $^1\Pi$ state, we used the reduced mass of NaD to solve the Hamiltonian equations with the NaH potential energy curve provided by Aymar et al.[19] We ignored the isotope shift in our calculations. The expected PQR line positions of the NaD *B* $^1\Pi \leftarrow X\ ^1\sum^+$ transitions were calculated with reference to the works of Chu et al.[4] ($X\ ^1\sum^+$ state) and Aymar et al.[19] (*B* $^1\Pi$ state). However, no significant signals were obtained. The results of the Franck–Condon calculations indicated that the Franck–Condon factors (FCFs) for transitions between the NaD *B* $^1\Pi$ state and the thermally populated ground state (v'' = 0 and 1) were too small (see the Supporting Information for details); therefore, the excitation signals were too weak for our experiments to detect.

3.2. Dispersed LIF and OODR Spectra. The assignment of the rotational quantum number *J* to the PQR lines of the NaH *B* state excitation spectrum was verified by the LIF spectra and OODR results. In laser spectroscopy, laser-induced fluorescence physically means the red shift of the original laser light source. Here, we used the originally recorded wavelength in the *x*-axis to draw the figures. The monochromator was scanned with a fixed-wavelength pump laser to record the LIF spectra. Figure 6 presents the excited state *B* (0, 5) LIF spectra of the *R*4 (middle panel, excited from *X* (0, 4)) and *P*6 (upper panel, excited from *X* (0, 6)) lines, and the lower panel presents the calculated LIF line positions with relevant Hönl–London rotational line strength factors (HLFs), which consisted of a series of *PR* pairs from the excited state *B* (0, 5) to the ground state *X* (v'', 4/6). The insets of Figure 6 (upper and middle panels) indicate that some parts of the LIF spectra had less interference from Na_2 fluorescence, and a lower scanning rate of 0.05 nm/step was used for these parts. These observations of LIF emission bands clearly matched the calculated LIF line positions as well as the HLFs.

Figure 7 shows the excited state *B* (0, 5) LIF spectrum of the *Q*5 line [upper panel, excited from *X* (0, 5)], and the lower panel presents the calculated LIF line positions with relevant HLFs multiplied by FCFs, which consisted of a series of emissions from the excited state *B* (0, 5) back to the ground

https://doi.org/10.1021/acsomega.1c02767
ACS Omega 2021, 6, 20629–20636

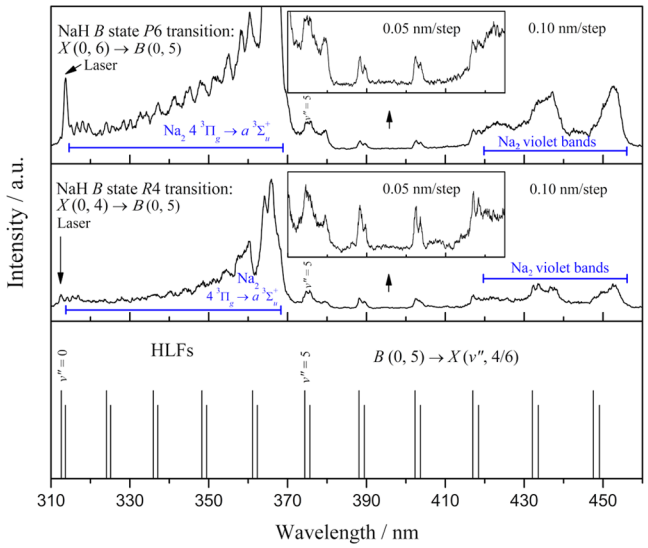

Figure 6. Upper panel: LIF spectrum of the *P*6 transition in the NaH *B* state. Middle panel: LIF spectrum of the *R*4 transition in the NaH *B* state. Lower panel: predicted fluorescence peak positions of the *B* (0, 5) → *X* (*v*″, 4/6) transitions. The relative peak intensities indicate the Hönl−London line strength factors for the *P*6 and *R*4 transitions. Insets: spectra obtained at a lower scanning rate of 0.05 nm/step.

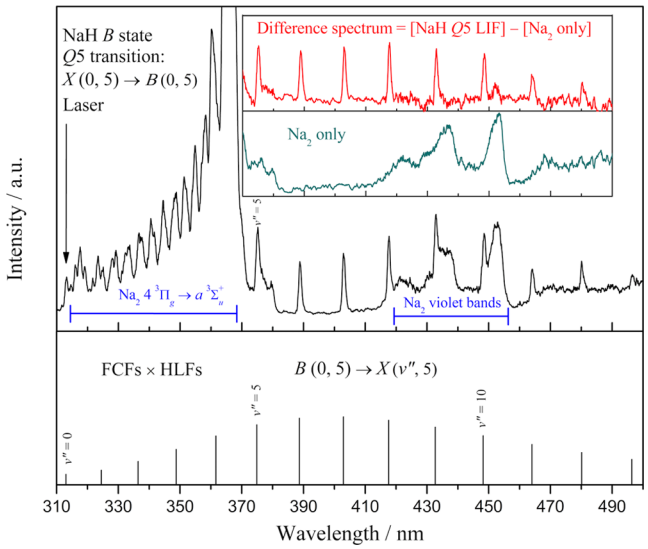

Figure 7. Upper panel: LIF spectrum of the NaH *B* state's *Q*5 transition. Lower panel: predicted fluorescence peak positions of the *B* (0, 5) → *X* (*v*″, 5) transitions. The relative peak intensities represent the Franck−Condon factors multiplied by the Hönl−London factors in the *Q*5 transition. Upper inset: difference spectrum after elimination of the interference signal of Na_2. Lower inset: LIF spectrum of the off-resonance NaH *B* state excitation.

state *X* (*v*″, 5). The upper inset of Figure 7 presents the difference spectrum that was observed after subtraction of the fluorescence spectrum of the sodium dimer (see the lower inset of Figure 7), which was obtained from setting the pump laser wavelength at an off-resonance position for the NaH molecule. The difference spectrum reveals clear LIF emission bands matching the calculated LIF line positions and reveals the trend of the HLFs multiplied by the FCFs.

The interference of Na_2 fluorescence had a substantial effect on the investigation of the NaH *B* $^1\Pi$ state. As illustrated in Figures 6 and 7, strong fluorescence signals were observed in the spectral ranges of 315−370 and 420−455 nm that originated from the Na_2 4 $^3\Pi_g \rightarrow a\ ^3\sum_u^+$ emission[32−34] and the Na_2 violet diffuse bands,[35−39] respectively. To avoid the interference of Na_2 fluorescence, a color filter was not used to obtain the laser-induced excitation spectrum of the NaH *B* state; instead, a monochromator−photomultiplier combination was used in the wavelength range of 380−410 nm. The monochromator was set to 388 or 403 nm for detecting the fluorescence of the $B\ ^1\Pi \rightarrow X\ ^1\sum^+$ transitions, with slit widths of 1.5−3.0 mm. This approach was favorable for the pump laser frequencies of 31 700−32 200 cm^{-1} that corresponded to the *B* (0, *J*) ← *X* (0, *J*″) transitions (see Figure 3). However, among the *B* (0, *J*) ← *X* (1, *J*″) transitions with pump laser frequencies of 30 600−31 100 cm^{-1}, the LIF spectrum had stronger Na_2 fluorescence interference in the wavelength range of 380−410 nm (see the Supporting Information for details). This meant that Na_2 fluorescence interference could not be prevented in the excitation spectrum. One method of solving this problem is performing difference spectral analysis (see Figure 4), the results of which indicate whether spectroscopy analysis should be performed.

Supporting evidence for our assignment of the rotational quantum number *J* can also be provided by OODR spectroscopy because this advantageous technique has rigorous state selectivity. The experimental setup for OODR spectroscopy has been described in detail elsewhere.[3,4,7,8] The V-type OODR was used to confirm our *J* assignment. Figure 8

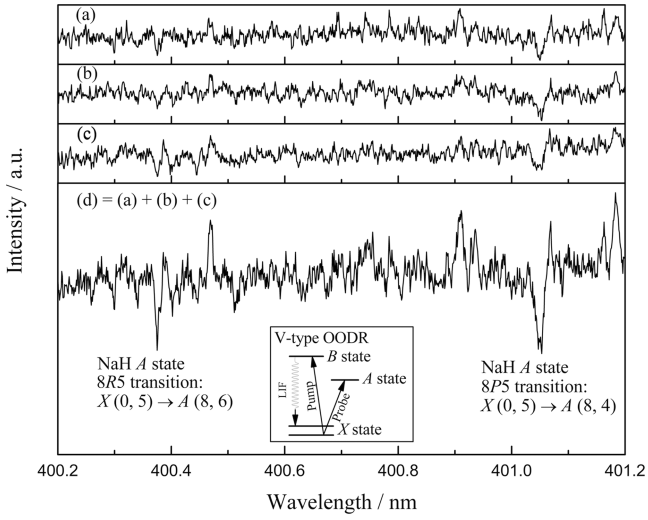

Figure 8. (a−c) V-type OODR fluorescence depletion spectra obtained from multiple measurements. (d) To obtain the OODR spectrum, three duplicate measurements were combined. Inset: experimental scheme for the OODR fluorescence depletion technique.

illustrates the V-type OODR fluorescence depletion spectra with a common lower-level *X* (0, 5). A pump laser was used for selective excitation of the NaH *B* state *Q*5 transition *B* (0, 5) ← *X* (0, 5), and a selective LIF emission *B* (0, 5) → *X* (6, 5) was monitored with a combined monochromator and photomultiplier. The probe laser was tuned for the spectral range of interest, which included the NaH *A* $^1\sum^+$ state *P*5 and *R*5 transitions at the vibrational level *v*′ = 8 (the term energies and assignments of the *A* state were taken from another study[6]). Some peaks enhanced by fluorescence due to NaH *A*

https://doi.org/10.1021/acsomega.1c02767
ACS Omega 2021, 6, 20629−20636

Table 2. Molecular Constants for the NaH $B\ ^1\Pi$ State[a]

	this work (v = 0)						
constant	$B\ ^1\Pi^+$	$B\ ^1\Pi^-$	$B\ ^1\Pi$[b]	Aymar et al.[c]	Khelifi[d]	Yang et al.[e]	Olson et al.[f]
Y_{00}	32613.879(146)	32614.231(238)	32613.997(124)				
Y_{01}	2.038(11)	2.024(18)	2.034(9)			2.2669	
$Y_{02} \times 10^3$	−1.795(151)	−1.701(247)	−1.764(129)			−1.4003	
ω	137.36(19)	139.64(30)	138.09(16)	214		182.42	
D_0	169(6)	169(6)	169(6)			145.72	
D_e	238(6)	239(7)	238(6)	282	1081.77	226.23	120.98
$\langle R\rangle$ or R_e (Å)	2.927(8)[g]	2.937(13)[g]	2.930(7)[g]	2.70	2.39	2.7752	2.80

[a]All values are expressed in cm^{-1} unless otherwise indicated. [b]Dunham fitting of all of the experimental data for the vibrational quantum number v = 0. [c]Ref 19. [d]Ref 18. [e]Ref 17. [f]Ref 13. [g]$R = (2\mu B_v)^{-1/2}$.

$^1\sum^+ \rightarrow X\ ^1\sum^+$ emission were observed. The inset of Figure 8 illustrates the three lower-lying electronic states of NaH (X, A, and B states), including the experimental scheme we used. To emphasize the depletion signals, three duplicate results were combined, as illustrated in Figure 8d. Unambiguous assignments of the A (8, 4/6) ← X (0, 5) transitions from previous work demonstrated that our J assignment was correct.

3.3. Molecular Constants. The observed rovibrational levels of the NaH $B\ ^1\Pi$ state contained eight e-parity and eight f-parity sublevels (v = 0, J = 1−8), including a total of 48 transitions (see Table 1 and the Supporting Information). Three Dunham-type coefficients were used to fit the observed term values, and the Dunham expansion is as follows[1,40]

$$T(0, J) = Y_{00} + Y_{01}[J(J+1) - 1] + Y_{02}[J(J+1) - 1]^2 \quad (1)$$

Table 2 contains a summary of the fitting results with standard deviations in parentheses, including the NaH $B\ ^1\Pi^+$, $B\ ^1\Pi^-$, and $B\ ^1\Pi$ (fitting both e and f sublevels) states of v = 0 with their standard deviations of 0.39, 0.45, and 0.41 cm^{-1}, respectively. Details of the fitting results are included in the Supporting Information.

The mean internuclear distance ($\langle R\rangle$) was calculated according to the relation $R = (2\mu B_v)^{-1/2}$, where the rotational constant $B_v = Y_{01}$. Using the derived coefficient Y_{01} and the reduced mass μ = 0.9654995 amu[41] of NaH, we determined that the $\langle R\rangle$ values were 2.927(8), 2.937(13), and 2.930(7) Å for the $B\ ^1\Pi^+$, $B\ ^1\Pi^-$, and $B\ ^1\Pi$ states, respectively. Table 2 contains a summary of the $\langle R\rangle$ values and the theoretical equilibrium internuclear distance R_e obtained from the literature.[13,17−19]

Using the centrifugal distortion relation $D = 4B^3/\omega^2$ for estimating the value of the vibrational frequency ω, under the assumption that $B = Y_{01}$ and $D = Y_{02}$, we calculated the ω values to be 137.36(19), 139.64(30), and 138.09(16) cm^{-1} for the $B\ ^1\Pi^+$, $B\ ^1\Pi^-$, and $B\ ^1\Pi$ states, respectively. Table 2 presents these values and theoretical ω_e values of 182.42 cm^{-1} reported by Yang et al.[17] and 214 cm^{-1} reported by Aymar et al.[19]

Using the term energies of $T\ (0, 1)_e$ = 32615.916 cm^{-1}, $T\ (0, 1)_f$ = 32616.253 cm^{-1}, and $T\ (0, 1)$ = 32616.028 cm^{-1} and the asymptotic energy $Na(3\ ^2P_{3/2}) + H(1\ ^2S_{1/2})$ = 32 785(6) cm^{-1}, we determined that the dissociation energy D_0 had the same value of 169(6) cm^{-1} for the $B\ ^1\Pi^+$, $B\ ^1\Pi^-$, and $B\ ^1\Pi$ states. However, the zero-point energy (ZPE), where ZPE = $\omega/2 - \omega x/4$,[42] could be estimated if it is assumed to be approximately $\omega/2$; using this knowledge, the dissociation energies D_e, in which $D_e = D_0$ + ZPE, were then estimated to be 238(6), 239(7), and 238(6) cm^{-1} for the $B\ ^1\Pi^+$, $B\ ^1\Pi^-$, and $B\ ^1\Pi$ states, respectively. Table 2 summarizes the dissociation energies together with other studies' reported theoretical D_e values of 120.98,[13] 226.23,[17] 1081.77,[18] and 282 cm^{-1}.[19]

4. CONCLUSIONS

The NaH $B\ ^1\Pi$ state was observed for the first time using pulsed LIF excitation spectroscopy. Because of poor Franck−Condon overlap, only one vibrational level was observed in this study. A total of 24 B ($0, J$) ← X ($0, J''$) and 24 B ($0, J$) ← X ($1, J''$) transitions were observed, including eight e-parity and eight f-parity sublevels of a series of PQR lines. The eigenvalues we obtained by solving Hamiltonian equations with the *ab initio* potential curve[19] were shifted by a constant to match the observed rovibrational levels and were in excellent agreement with the experimental results. Thus, the observed vibrational level was assigned to be v = 0. The assignment of the rotational quantum number J was supported and verified by (a) comparison to the *ab initio* calculations, (b) the LIF spectrum, and (c) the results of OODR spectroscopy, which has rigorous state selectivity. Values were proposed for the Dunham-type coefficients, mean internuclear distance ($\langle R\rangle$) for v = 0, the vibrational frequency ω, and dissociation energies D_0 and D_e.

■ ASSOCIATED CONTENT

Supporting Information

The Supporting Information is available free of charge at https://pubs.acs.org/doi/10.1021/acsomega.1c02767.

Observed transitions (Table S1), FCFs and predicted transition bands (NaH) (Table S2), FCFs and predicted transition bands (NaD) (Table S3), Dunham fitting (e sublevels, NaH) (Table S4), Dunham fitting (f sublevels, NaH) (Table S5), and Dunham fitting (all sublevels, NaH) (Table S6) (PDF)

■ AUTHOR INFORMATION

Corresponding Authors

Chin-Chun Tsai − *Department of Physics, National Cheng Kung University, Tainan 70101, Taiwan*; Email: chintsai@mail.ncku.edu.tw

Thou-Jen Whang − *Department of Chemistry, National Cheng Kung University, Tainan 70101, Taiwan*; orcid.org/0000-0003-0111-7107; Email: twhang@mail.ncku.edu.tw

Authors

Chia-Ching Chu − *Department of Chemistry, National Cheng Kung University, Tainan 70101, Taiwan*

https://doi.org/10.1021/acsomega.1c02767
ACS Omega 2021, 6, 20629−20636

Chun Huang − *Department of Chemistry, National Cheng Kung University, Tainan 70101, Taiwan*

Complete contact information is available at: https://pubs.acs.org/10.1021/acsomega.1c02767

Notes

The authors declare no competing financial interest.

■ ACKNOWLEDGMENTS

We gratefully acknowledge the support of the Ministry of Science and Technology, Taiwan under Grant Nos. MOST 107-2113-M-006-007 and MOST 109-2113-M-006-012. C.-C.C. acknowledges the careful reading and helpful suggestions on details of the manuscript provided by Rui-En Hsu.

■ REFERENCES

(1) Herzberg, G. In *Molecular Spectra and Molecular Structure, Spectra of Diatomic Molecules*, 2nd ed.; Robert, E., Ed.; Krieger Publishing Co: Malabar, FL, 1989; Vol. *1*.

(2) Stwalley, W. C.; Zemke, W. T.; Yang, S. C. Spectroscopy and Structure of the Alkali Hydride Diatomic Molecules and Their Ions. *J. Phys. Chem. Ref. Data* **1991**, *20*, 153−187.

(3) Huang, H. Y.; Lu, T. L.; Whang, T. J.; Chang, Y. Y.; Tsai, C. C. Dissociation Energy of the Ground State of NaH. *J. Chem. Phys.* **2010**, *133*, No. 044301.

(4) Chu, C. C.; He, W. F.; Lin, R. S.; Li, Y. J.; Whang, T. J.; Tsai, C. C. Spectroscopic Determination of the Ground-state Dissociation Energy and Isotopic Shift of NaD. *J. Chem. Phys.* **2017**, *147*, No. 024301.

(5) Lochbrunner, S.; Motzkus, M.; Pichler, G.; Kompa, K. L.; Hering, P. New Dunham Coefficients of the A $^1\sum^+$-state of NaH and NaD. *Z. Phys. D: At., Mol. Clusters* **1996**, *38*, 35−40.

(6) Pesl, F. P.; Lutz, S.; Bergmann, K. Improved Molecular Constants for the X $^1\sum^+$ and A $^1\sum^+$ States of NaH. *Eur. Phys. J. D* **2000**, *10*, 247−257.

(7) Huang, H. Y.; Chang, Y. Y.; Liao, M. H.; Wu, K. L.; Lu, T. L.; Chang, Y. Y.; Tsai, C. C.; Whang, T. J. Characterization of the Outer Well of NaH C $^1\sum^+$ State by Fluorescence Depletion Spectroscopy. *Chem. Phys. Lett.* **2010**, *493*, 53−56.

(8) Chu, C. C.; Huang, H. Y.; Whang, T. J.; Tsai, C. C. Observation of Double-well Potential of NaH C $^1\sum^+$ State: Deriving the Dissociation Energy of Its Ground State. *J. Chem. Phys.* **2018**, *148*, No. 114301.

(9) Lewis, E. L.; McNamara, L. F.; Michels, H. H. Broadening of the Sodium D Lines by Atomic Hydrogen. An Analysis in Terms of the NaH Molecular Potentials. *Phys. Rev. A* **1971**, *3*, 1939−1948.

(10) Sachs, E. S.; Hinze, J.; Sabelli, N. H. Frozen Core Approximation, a Pseudopotential Method Tested on Six States of NaH. *J. Chem. Phys.* **1975**, *62*, 3393−3398.

(11) Numrich, R. W.; Truhlar, D. G. Mixing of Ionic and Covalent Configurations for NaH, KH, and MgH^+. Potential Energy Curves and Couplings between Molecular States. *J. Phys. Chem. A* **1975**, *79*, 2745−2766.

(12) Melius, C. F.; Numrich, R. W.; Truhlar, D. G. Calculations of Potential Energy Curves for the Ground States of NaH^+ and KH^+ and Π States of NaH and KH. *J. Phys. Chem. B* **1979**, *83*, 1221−1227.

(13) Olson, R. E.; Liu, B. Interaction Energies for Low-lying Electronic States of NaH and NaH^-: Scattering of H^- by Alkali Atoms. *J. Chem. Phys.* **1980**, *73*, 2817−2824.

(14) Olson, R. E.; Kimura, M. Molecular-state Cross-section Calculations for H + Na ⇄ H^- + Na^+. *Phys. Rev. A* **1985**, *32*, 3092−3094.

(15) Belyaev, A. K.; Grosser, J.; Hahne, J.; T, M. Ab Initio Cross Sections for Low-energy Inelastic H + Na Collisions. *Phys. Rev. A* **1999**, *60*, 2151−2158.

(16) Leininger, T.; Gadéa, F. X.; Dickinson, A. S. Broadening of the Sodium 568.8, 589, 615.4 and 819.4 nm Lines by Atomic Hydrogen. *J. Phys. B: At., Mol. Opt. Phys.* **2000**, *33*, 1805−1817.

(17) Yang, C. L.; Zhang, X.; Han, K. L. Analytical Potential Energy Function and Spectroscopic Parameters for the Ground and Excited States of NaH. *J. Mol. Struct.: THEOCHEM* **2004**, *676*, 209−213.

(18) Khelifi, N. Theoretical Study of the $^{1,3}\sum^+$ States of the NaH Molecule in the Adiabatic and Diabatic Representations. *J. Russ. Laser Res.* **2008**, *29*, 274−287.

(19) Aymar, M.; Deiglmayr, J.; Dulieu, O. Systematic Trends in Electronic Properties of Alkali Hydrides. *Can. J. Phys.* **2009**, *87*, 543−556.

(20) Vahala, L.; Havey, M. D. Systematic Estimate of Binding Energies of Weakly Bound Diatomic Molecules. *J. Chem. Phys.* **1984**, *81*, 4867.

(21) Lemeshko, M.; Friedrich, B. Rotational and Rotationless States of Weakly Bound Molecules. *Phys. Rev. A* **2009**, *79*, No. 050501.

(22) Amore, P.; Fernández, F. M.; Jiménez, E. Weakly (and Not So Weakly) Bound States of a Relativistic Particle in One Dimension. *Phys. Lett. A* **2018**, *382*, 2097−2102.

(23) Willner, K. Theoretical Study of Weakly Bound Vibrational States of the Sodium Trimer: Numerical Methods; Prospects for the Formation of Na_3 in Anultracold Gas. Ph.D. Thesis, Université Paris Sud - Paris XI: Paris, 2005.

(24) Laue, T.; Tiesinga, E.; Samuelis, C.; Knöckel, H.; Tiemann, E. Magnetic-Field Imaging of Weakly Bound Levels of the Ground-State Na_2 Dimer. *Phys. Rev. A* **2002**, *65*, No. 023412.

(25) Chu, C. C.; Huang, H. Y.; Lin, H. C.; Hsiao, Y. H.; Whang, T. J.; Tsai, C. C. Observation of the Shallow 2 ^{1}Π State of NaH. *J. Chem. Phys.* **2019**, *150*, No. 024303.

(26) Lee, A. Y.; Luh, W. T. Spectroscopic Study of the B ^{1}Π State of ^{39}KH. *J. Chem. Phys.* **2009**, *131*, No. 164304.

(27) Velasco, R. Ultraviolet Spectra of LiH and LiD. *Can. J. Phys.* **1957**, *35*, 1204−1214.

(28) Luh, W. T.; Kleiber, P. D.; Lyyra, A. M.; Stwalley, W. C.; Lin, K. C. Laser-Induced Fluorescence of the B ^{1}Π-X $^1\sum^+$ Band System of the Isotopic Lithium Hydrides. *J. Mol. Spectrosc.* **1988**, *129*, 388−394.

(29) Saloman, E. B.; Sansonetti, C. J. Wavelengths, Energy Level Classifications, and Energy Levels for the Spectrum of Neutral Neon. *J. Phys. Chem. Ref. Data* **2004**, *33*, 1113−1158.

(30) Demtröder, W. *Laser Spectroscopy*, 1st ed.; Springer-Verlag: Berlin, 1981; pp 124−169.

(31) Sansonetti, J. E. Wavelengths, Transition Probabilities, and Energy Levels for the Spectra of Sodium (Na I−Na XI). *J. Phys. Chem. Ref. Data* **2008**, *37*, 1659−1763.

(32) Liu, Y. M.; Chen, H. M.; Li, J.; Chen, D. Y.; Li, L.; Field, R. W. The 4 $^3\Pi_g$ and 6 $^3\Pi_g$ States of Na_2: Observation and Assignment. *J. Mol. Spectrosc.* **1998**, *192*, 32−40.

(33) Lazarov, G.; Lyyra, A. M.; Li, L.; Huennekens, J. The 4 $^3\Pi_g$ State of Na_2: Vibrational Numbering and Hyperfine Structure. *J. Mol. Spectrosc.* **1999**, *196*, 259−264.

(34) Ivanov, V. S.; Sovkov, V. B.; Gallice, N.; Li, L.; Liu, Y.; Lyyra, A. M.; Magnier, S. Use of Bound−Free Structured Spectra in Determining RKR Potentials: The 4 $^3\Pi_g$ State of Na_2. *J. Mol. Spectrosc.* **2001**, *209*, 116−121.

(35) Woerdman, J. P. Doppler-free Two-photon Transitions of the Sodium Molecule. *Chem. Phys. Lett.* **1976**, *43*, 279−282.

(36) Woerdman, J. P. Laser-excited Broadband Violet Emission from Sodium Molecules. *Opt. Commun.* **1978**, *26*, 216−218.

(37) Bahns, J. T.; Stwalley, W. C. Observation of Gain in the Violet Bands of Sodium Vapor. *Appl. Phys. Lett.* **1984**, *44*, 826−828.

(38) Pichler, G.; Bahns, J. T.; Sando, K. M.; Stwalley, W. C.; Konowalow, D. D.; Li, L.; Field, R. W.; Müller, W. Electronic Assignments of the Violet Bands of Sodium. *Chem. Phys. Lett.* **1986**, *129*, 425−428.

(39) Xing, D.; Wang, Q.; Tan, S.; Ueda, K. Triplet-state Bound-free Transitions of Alkali Dimers (Na_2, K_2, and Rb_2) by Electron-beam Excitation. *IEEE J. Quantum Electron.* **1998**, *34*, 1765−1771.

(40) Dunham, J. L. The Energy Levels of a Rotating Vibrator. *Phys. Rev.* **1932**, *41*, 721−731.
(41) Walji, S. D.; Sentjens, K. M.; LeRoy, R. J. Dissociation Energies and Potential Energy Functions for the Ground X $^1\sum^+$ and "Avoided-Crossing" A $^1\sum^+$ States of NaH. *J. Chem. Phys.* **2015**, *142*, No. 044305.
(42) Irikura, K. K. Experimental Vibrational Zero-Point Energies: Diatomic Molecules. *J. Phys. Chem. Ref. Data* **2007**, *36*, 389−397.

https://doi.org/10.1021/acsomega.1c02767
ACS Omega 2021, 6, 20629−20636